Determinant morphological features of flax plant products and their contribution in injection moulded composite reinforcement

Lucile Nuez, Maxime Gautreau, Claire Mayer-Laigle, Pierre d'Arras, Fabienne Guillon, Alain Bourmaud, Christophe Baley, Johnny Beaugrand

Composites Part C: Open Access 3 (2020) 100054

Contents lists available at ScienceDirect

Composites Part C: Open Access

journal homepage: www.elsevier.com/locate/jcomc

Determinant morphological features of flax plant products and their contribution in injection moulded composite reinforcement

Lucile Nuez[a,b,*], Maxime Gautreau[c], Claire Mayer-Laigle[d], Pierre D'Arras[b], Fabienne Guillon[c], Alain Bourmaud[a], Christophe Baley[a], Johnny Beaugrand[c]

[a] Université de Bretagne-Sud, IRDL, CNRS UMR 6027, BP 92116, 56321 Lorient Cedex, France
[b] Van Robaeys Frères, 83 Rue Saint-Michel, 59122 Killem, France
[c] Biopolymères Intéractions Assemblages (BIA), INRAE, Rue de la Géraudière, F-44316 Nantes, France
[d] IATE, Univ Montpellier, CIRAD, INRAE, Montpellier SupAgro, Montpellier, France

ARTICLE INFO

Keywords:
Fibres
Shives
Dust
Fines
Morphometric characterisation
Injection moulding
Carbohydrate analysis

ABSTRACT

The use of biomass in injection moulded or extruded thermoplastic composites is an important issue, especially when trying to add value to low-cost co-products. The objective of this work was to conduct a complete study on the morphological characterisation and carbohydrate analysis of a range of co-products obtained during the processing of flax straw. Thus, the morphology of *(i)* cut flax fibres, *(ii)* fragmented shives, and *(iii)* scutching and carding dusts is characterised using a dynamic image analyser with a sieving approach. These different fractions are then used to produce injection moulded composite materials. Their mechanical performances are discussed in relation to the morphology of the reinforcements, as well as their carbohydrate compositions and fine particle contents. Co-products, based on their reinforcement properties, can be classified into three categories. In all cases, a reinforcing effect is demonstrated for the tensile Young's modulus with an increase from +24 to +137% depending of the material. A linear relationship was observed between the cellulose content of reinforcing material and the tensile strength at break of the injection moulded composites. The results are promising for adding value to all flax co-products in plastics processing, targeting industrial applications in line with their intrinsic performances.

Introduction

Flax fibre reinforced composites are now present in different industrial sectors and are the subject of numerous academic and industrial developments. Flax (*linum usitatissimum L.*), when cultivated for its fibres, offers various by-products, particularly *(i)* the most added-value bast fibres, *(ii)* flax shives originating from the xylem of the stem, as well as *(iii)* dusts induced by the manufacturing processing steps of fibre extraction and refining.

Short or cut fibres (< 5 mm) are used for composite materials that are generally extruded or injection moulded [1]. The morphological characterisation of the plant reinforcements used to produce these composite materials is a crucial point for a range of reasons [2]: these data are essential to evaluate the tensile properties of the manufactured composites, the fibre-matrix adhesion, or fibre packing, all of which are necessary for modelling studies and behaviour analysis, where it is important to consider the morphology of the reinforcements and their dispersion, particularly in the case of thermoplastic composites obtained via compounding [3]. The length and diameter of the reinforcements are two main parameters necessary to estimate their reinforcing capacity in a composite material [4]; they are assessed by the value of the aspect ratio, which represents the length of the fibrous element divided by its diameter. This aspect ratio allows to determine the efficiency of the load transfer between the reinforcement and the matrix. In the case of flax fibres, retting and extracting conditions particularly affect the diameter of the fibre bundles and therefore have a direct impact on their aspect ratio [5]. The aspect ratio also depends on the tools used to manufacture the composite parts [3]. The wide range of shear rates that possibly occur in plastics processing is also a criterion for selecting the best processes to preserve the integrity of plant fibres. In addition, in the case of injection moulded or extruded parts, it has been shown that, depending on the nature of the process or the number of cycles, a greater or lesser quantity of fine particles (particles of less than 200 μm) may be present in the materials [6]. These elements can degrade the mechanical performance of the parts in a significant way and being able to quantify them is important [7].

The morphological analysis of reinforcements is accessible by different means, including laser diffraction methods, static or dynamic image

* Corresponding author at: Université de Bretagne-Sud, IRDL, CNRS UMR 6027, BP 92116, 56321 Lorient Cedex, France.
E-mail address: lucile.nuez@univ-ubs.fr (L. Nuez).

https://doi.org/10.1016/j.jcomc.2020.100054
Received 7 August 2020; Received in revised form 21 October 2020; Accepted 22 October 2020

analysis. They depend on numerous parameters, such as the analysis method, the resolution of each equipment, the ability to obtain a statistically representative sample, the morphological complexity of the particles, etc.

Laser diffraction methods are based on the light diffraction of particles, which depends on their size. This technique is generally accurate for small particles, and while it allows for high speed analysis, it highly depends on the optical model which is necessary to mathematically transform the particle scatter intensity into a size distribution. Optical models such as the Fraunhofer approximation of the Mie scattering theory are based on several assumptions, such as spherical particles [8].

Static image analysis is based on particles positioned on a slide before inspection by a camera or microscope, followed by an image analysis method requiring a thresholding step (separation of particles from their background) before further analysis. Examples of static image analysis methods include microscopy or scanner measurements, which can be performed in combination with manual image analysis or using specific software such as FibreShape. Nevertheless, these static analysis techniques are time-consuming, they often neglect the smallest particles [9], and only slight variations were measured between these methods and laser-based dimensional analysis [10,11].

For dynamic image analysis, particles flow in front of a recording camera that captures their shadows at a wanted frequency and that are then automatically analysed in a similar manner as static image analysis. Furthermore, the use of automatic systems allows to gain time and the number of analysed particles can rise up to several tens of thousands of objects in less than one minute [12], such as with the QICPIC [13], or with the MorFi Compact® fibre analyser, which is a specific automatic equipment initially developed for the paper industry before or after a process stage that has been used in different studies [6,14–16]. The fibres circulate in a water or ethanol bath and image acquisitions allow for lengths of several mm to be analysed, but the relatively low camera resolution is penalising for single fibre diameter measurements. However, this method has the advantage of reliably quantifying fine particles (less than 200 μm) whose number fraction increases significantly after injection or extrusion cycles [6]. Other automated measurement instruments designed for cellulose fibre analysis by polarised light diffraction include the FS-200 or the Fibre Quality Analyser (FQA) [17–19]. The lenses used, the depth of focus and the focusing difficulties associated must also be taken into consideration, depending on the specificities of the sample to be analysed. The choice of a measuring technique is therefore a compromise between what needs to be analysed and the current available techniques.

The aim of this paper is to measure the relevant parameters of a range of flax co-products that can be used as injection moulded composite reinforcements. We focus on the characterisation of hackled fibres, fragmented shives and even scutching and carding dusts, i.e., the overall flax products representative of the entire flax stem. Their uses, length, individualisation, aspect ratio or presence of a heterogeneous population of components, morphologically speaking, are quantified using a dynamic morphological analyser. The results obtained are then analysed in relation to the structure, carbohydrate analysis, and origin of these different flax plant fractions; then their use in poly-(propylene) injection moulded composites is mechanically tested and analysed. These data make it possible to fully understand the specificities of each flax co-product and consider their interest for composite material reinforcement applications.

Experimental procedure

Flax products

Cut flax fibres

The flax fibre is from the Alizée variety, which was harvested in 2017 in Normandy, supplied and cut by Depestele (Bourguebus, France); flax stems were pulled out, dew retted for 6 weeks and then scutched and hackled. The resulting fibres were then industrially cut to 1, 2 and 4 mm in length, and respectively named FF1, FF2 and FF4. In the rest of this study, the term “fibre” will designate both elementary fibres and flax fibre bundles, as both are present in the three studied batches; otherwise differentiation will be made by specifying “elementary fibres” or “bundles”. The samples names and processing are supplied in Fig. 1.

Flax shives

The flax shives (FS) were provided in bulk by the flax scutching company Van Robaeys Frères (France), following the scutching of the 2018 flax harvest year, before being milled with a laboratory scale rotating cutting mill (Retsch Mühle, Germany). The mesh size of the grid used was 500 μm, accounting for sample B500. The latter, after being previously oven dried at 60 °C, was then further fractionated by sieve separation using a vibrating sieving column (Proviteq, France) composed of 5 sieves with square mesh sizes of 630, 400, 315, 100 and 50 μm, and completed with a bottom sieve. The sample names and methods of obtention are summarised in Fig. 1.

Scutching and carding dust

Scutching and carding dusts were provided by the flax scutching company Van Robaeys Frères (France). The scutching dusts (SD) were retrieved from the condensers in the air vacuuming system, especially during the retted flax bale unrolling process in the scutching line, and more globally along each step of the scutching process. Similarly, the carding dusts (CD) were obtained during the refining process of the flax tows or “short” fibres obtained as co-products during the scutching [20] transformation step, which consists of carding and further refining. Sample names and means of production are shown Fig. 1. The SD and CD were fractionated via sieve separation using a vibrating sieving column (Retsch, Germany) composed of 5 sieves with square mesh sizes of 500, 250, 180, 125 and 90 μm, and completed with a bottom sieve.

Particle size analysis

Particle morphology was studied by a dynamic image analysis device, QICPIC (SympaTec GmbH, Germany). This equipment was chosen, since it must be able to evaluate the length of a variety of particles (from the size of fines to that of flax shives of varying diameters and of flax fibre elements of different lengths). Each sample has a substantial variability, so this technique is also able to measure a considerable number of particles to ensure its statistical representativity. Different protocols have been adapted for the particle’s morphometric description. Because of a tendency to particle aggregation, the flax shives (both fragmented and sieved portions), the cut fibres, and the scutching and carding dust samples were dispersed in liquid using a unit adapted to the device, LIXCEL, which provides both ultrasonic agitation and stirring at the same time. Each sample was weighed to approximately 50 mg and dispersed first in 5 mL of ethanol and 45 mL of distilled water, before the final dispersion in 950 mL of water with a magnetic stirrer. The flax shives were analysed using the M7 lens specific to the QICPIC, which is appropriate for measuring particles of a length ranging from 4.2 μm at a minimum to 8665 μm at a maximum (ISO 13322-1/2). The cut flax fibre samples were analysed with the M9 lens, which is appropriate for particles ranging from 17 μm to 33,792 μm (ISO 13322-1/2) in order to compare the samples with one another.

The number of analysed particles varied between 39,000 and 2.8 million, depending on the samples and measurements, and were made in duplicates to ensure reproducibility of the results. PAQXOS software (SympaTec GmbH, Germany) was used to calculate, in real time, the particle length, defined as the shortest path between the most distant end points of the particles after skeletonisation (Lefi function). The particle diameter was calculated using the Difi function, defined as the division of the projected particle area by the sum of all branch length of the fibre skeleton. The particle aspect ratio was calculated as the opposite of the elongation parameter given by the PAQXOS software (defined as the

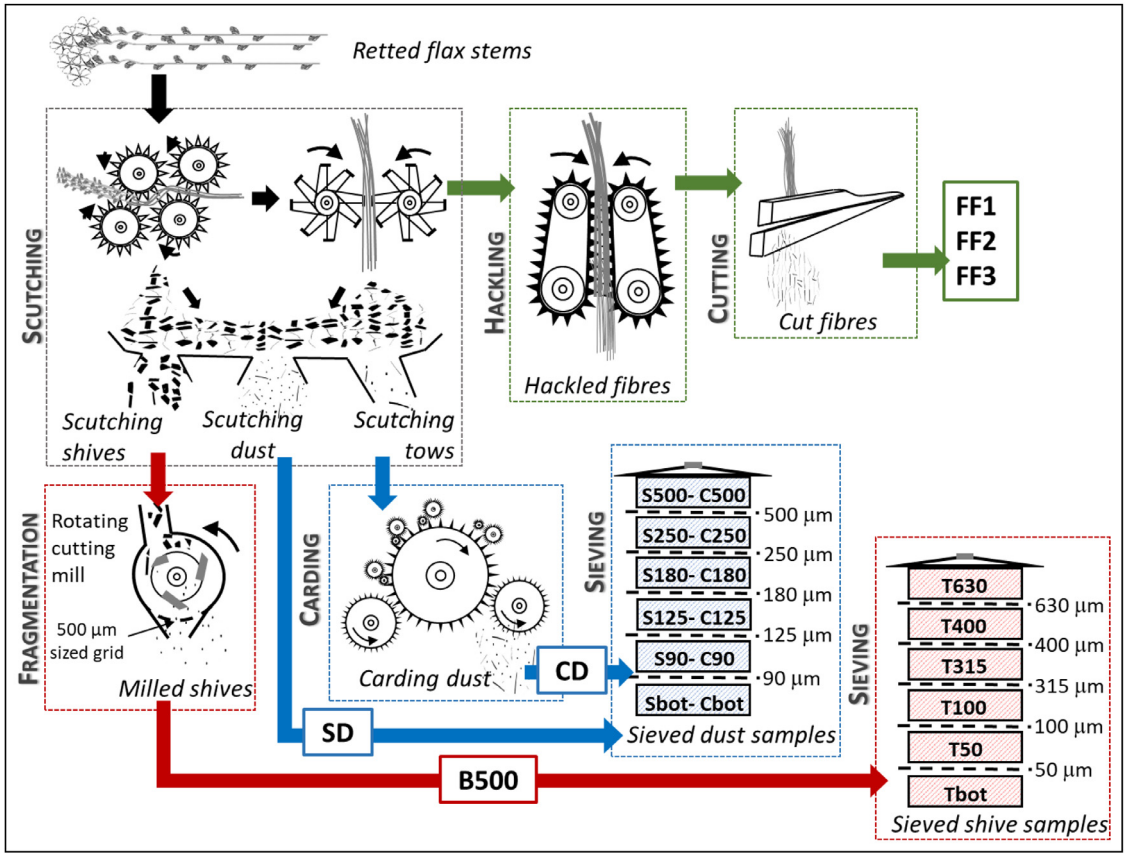

Fig. 1. Reinforcing material samples, their origin and corresponding processing steps used for isolation. FF1, FF2 and FF4 refer to the scutched and hackled flax fibres cut to 1, 2 and 4 mm, respectively; B500 refers to the fragmented flax shives; T630, T400, T315, T100, T50, and Tbot refer to its sieved fractions collected above the corresponding mesh sizes, and finally SD and CD refer to the scutching and carding dusts, respectively. S500, S250, S180, S125, S90 and Sbot, as well as C500, C250, C180, C125, C90 and Cbot, refer to their respective sieved fractions. The colour key is respected throughout this study for the main samples.

ratio of Difi and Lefi). Another morphological parameter, sphericity, is calculated to characterise the particles. Sphericity is defined as follows (Eq. (1)):

$$Sphericity = \frac{perimeter\ of\ the\ area\ equivalent\ circle}{perimeter\ of\ the\ particle\ projection} \quad (1)$$

The analysis was conducted on the basis of the volume distribution, where each particle is given a weight depending on the volume of a cylinder of a length and diameter equivalent to the dimensions of the particle. The distribution span is calculated following Eq. (2):

$$Span = \frac{90^{th}\ percentile - 10^{th}\ percentile}{50^{th}\ percentile} \quad (2)$$

Scanning electron microscopy (SEM) observations

Each sample was observed using a scanning electron microscope (Jeol JSM-IT500HR, Japan) after being sputter coated with a thin layer of gold in an Edwards Sputter Coater. The images were taken under x25 and x100 magnification. The SEM observations were followed by an elemental analysis using an energy dispersive X-ray analysis system (EDS) for the Tbot samples of scutching and carding dusts using a Jeol SDD JED-2300 analysis station on the previously cited SEM. The accelerating voltage for the latter was 5 kV.

Composite manufacture

Each category of flax co-products was used to manufacture poly-(propylene) (PP) reinforced injection moulded composites with a 30%-wt fraction for each, following an extrusion process. The polymer matrix used in this study was a PPC 10,642 (Total Petrochemicals, France) with an MFI of 44 g/10 min (230 °C- 2.16 kg). As a compatibiliser, a maleic anhydride modified PP (MAPP) was added to the formulation at the proportion of 4%-wt. The polymer used was Orevac CA 100 (Arkema, France) with an MFI of 10 g/10 min at 190 °C and 0.325 kg.

Before manufacturing, both the scutching and carding dusts, SD and CD, were oven dried at 60 °C for approximately 12 h. They were then compounded with a co-rotating twin-screw extruder (TSA, Italy) and injection moulded (Battenfeld BA800, Austria) into ISO 527-2 type 1B normalised specimens following the same process as described elsewhere [21]. The extrusion temperature profile went from 180 °C to 190 °C with a die temperature of 180 °C, and a constant barrel temperature of 190 °C was applied during injection, with a mould temperature of 30 °C. The manufacturing process of the samples produced with fragmented flax shives (B500) and flax fibres of 1 mm (FF1) was described in a previous study [21], as well as for the composites produced with 2 mm long flax fibres (FF2) and with talc [7].

Tensile test

Tensile testing was conducted on the injection moulded composite specimens following the ISO 527 standard. An MTS Synergie 1000RT machine was used. The tensile speed was 1 mm/min, the nominal length was 25 mm, and tests were performed in a controlled environment of 23 ± 2 °C and 50 ± 5% relative humidity. A minimum of five specimens were tested following conditioning during at least 24 h in the same conditions as during testing. A 10 kN sensor was mounted on the machine to measure the applied force on the specimen, while an extensometer

allowed for measuring the deformation during testing. A minimum of 5 specimens were tested per composite formulation.

Carbohydrate analysis

A wet chemical analysis was used to determine the monosaccharide content of each studied flax product material category. Due to their size and for the purposes of homogeneity, approximately 1 g of flax fibres was initially cryogrinded (SPEX 6700 freezer mill). Following this step, approximately 5 mg of each sample (fragmented flax shives, scutching and carding dusts) were pre-hydrolysed with 12 M H_2SO_4 (Sigma Aldrich, USA) for 2 h at 25 °C and then further hydrolysed in 1.5 M H_2SO_4 for 2 h at 100 °C. Individual neutral sugars (arabinose, rhamnose, fucose, glucose, xylose, galactose and mannose) were quantified after their derivatisation into alditol acetates. Liquid-gas chromatography (Perkin Elmer, Clarus 580, Shelton, USA) equipped with a DB 225 capillary column (J&W Scientific, Folsom, USA) was performed at 205 °C, using H_2 as the carrier gas, in order to analyse the alditol acetate derivatives [22]. A standard sugars solution and inositol as internal standard were used for calibration. Uronic acids (sum of galacturonic acid (GalA) and glucuronic acid (GlcA)) in acid hydrolyzates were quantified using the m-hydroxybiphenyl method [23]. Measures were performed in triplicate, and the results are expressed as a percentage of dry matter mass.

Ash content

Approximatively 2 g of scutching and carding dust sample (SD or CD) were first weighted (m_1) and dried in an oven at 130 °C for 90 min. After cooling they were weighed again to determine the dry mass (m_s). The water content (w) was calculated using Eq. (3):

$$w = 1 - \frac{m_s}{m_1} \tag{3}$$

In parallel, approximatively two other grams of samples were first weighed (m_2) and then pyrolyzed at 900 °C for 2 hrs following norm ISO 2171 with a Heraeus Thermo-line oven (Thermo Fischer Scientific, USA). The residual mass was weighted (m_r) after cooling in a desiccator to room temperature. The ash content on the dry material was calculated according to Eq. (4):

$$Ash = 100 * \frac{m_r}{m_2 * (1 - w)} \tag{4}$$

where *Ash* is a percentage, m_2 is the sample mass in grams, and m_r is the sample residual mass in grams, and w the water content. The experiments were conducted in duplicate and averaged.

Results and discussion

Morphological analysis

Cut flax fibres

Since the mean length value does not give any information on the distribution span and is not representative of a given sample, the results are presented in a box-plot diagram, as shown in Fig. 2a, with the 10th (first decile), 15th (first quartile), 50th (median), 85th (third quartile), and 90th (last decile) percentiles of the cumulative length distribution, moving from the bottom up. The arithmetic mean is additionally represented with a dot.

Fig. 2b shows a symmetric distribution for all the cut fibre samples, with a mean length equal to the median. The arithmetic mean length of the flax fibres is 973 ± 15 μm, 2046 ± 14 μm and 4044 ± 65 μm for FF1, FF2 and FF4, respectively, signifying a normal distribution for these three samples.

Fig. 3a represents the SEM observations of the cut flax fibres, where it is possible to see, for all samples, a homogeneous fibre length in the form of both elementary fibres and bundles. To complete this observation, the diagrams in Fig. 3b display the captured images of the fibres by the QICPIC during the dynamic image analysis. For all samples, the cut fibre length is fully consistent with the targeted value, but a non-negligible amount of very small particles, notably of fines (particles of less than 200 μm) is also present. This length distribution (Fig. 2b) furthermore validates the cutting method used, as the targeted lengths are reached with a relative error of less than 3% for all samples.

The diameter distribution of the cut flax fibre samples is given in Fig. 4a, with mean diameter values of 112.7 ± 3.6 μm, 162.8 ± 6.3 μm, and 180.3 ± 7.3 μm for FF1, FF2 and FF4, respectively. Indeed, the shearing stresses induced by the cutting process tend to individualise the fibre bundles [24,25]: the smaller the desired fibre length, the higher the shearing stresses and the more individualised the fibres. The small shoulder for diameters between 40 and 65 μm for each measured sample may be due to an analysis artefact linked to the chosen lens.

The aspect ratio, being the particle's length divided by its diameter, is a good indicator of the particle elongation and composite reinforcement potential. Fig. 4b shows an increase in both the fibre aspect ratio and the distribution span with the fibre length. The median aspect ratio increases from 8.2 to 13.0 and 23.8 for FF1, FF2 and FF4, respectively, while the distribution span increases by 1% and 17% when FF2 and FF4 are compared to FF1, respectively. This outcome is expected considering the eminent increase in the fibre length (the lengths of FF2 and FF4 are multiplied by two and by four when compared to FF1) with respect to the gradual increase of the samples' diameters [26].

Fragmented flax shives

Fig. 5a represents the length distribution of the fragmented flax shive sample B500, as well as its sieved fractions. The B500 sample presents an important span in the length distribution, with a mean length of 1262 ± 64 μm. This length is coherent when looking at the length distribution of each sieved fraction and when considering their corresponding mass fractions. The coarsest particles in sample T630 also present a wide length distribution with a mean particle length slightly higher than B500 at 1487 ± 45 μm. While the sieving step performed in this study might prove to be costly at an industrial scale, it emerges as a precious insight for understanding the variety of particle morphologies. The sieving mass fraction is given under each sieved sample (Fig. 5a). Sample T400 accounts for 62% of the initial B500 fragmented shives, together with samples T630 and T100, which each make up for 13% of the initial mass of B500. This percentage is surprisingly important for the T630 sample, regarding the fact that the rotating cutting mill grid mesh size was 500 μm. It can be explained by the agglomeration of longer particles during sieving that could prevent a portion of smaller particles to pass through the sieve, and thus cause an important distribution span. The remaining sieved fractions (T315, T50 and Tbot) sum up to 12% once added together. Therefore, the majority of the fragmented particles belong to the T400 sieved sample, thus they are the most present in terms of mass in B500. However, the morphologic characteristics of the cutting-milled B500 flax shive sample enclose those of each sieving fraction and were used as such for the composite reinforcement material (see Section 3.2).

The SEM observations of the flax shive sample (Fig. 5b–g), show the presence of the remaining fibres (both elementary and in the form of bundles), particularly for T630 (Fig. 5b) and T50 (Fig. 5f), together with large sized flax shive fragments. Fibres tend to agglomerate during sieving fractionation, which could explain why they are so importantly present in this fraction.

The following sieving fractions show a more restricted length distribution, with mean lengths at 1443 ± 2 μm, 1126 ± 8 μm, 920 ± 19 μm, 276 ± 1 μm and 106 ± 4 μm for the T400, T315, T100 and Tbot samples, respectively. Their SEM images (Fig. 5c–g) clearly show a reduction in the particle diameter with each sieve separation, with particles of relatively homogeneous lengths for samples T400 and T315, accounting both for a length distribution span of 0.8. In contrast, the length distribution span of the remaining samples gradually increases to 1.3 for

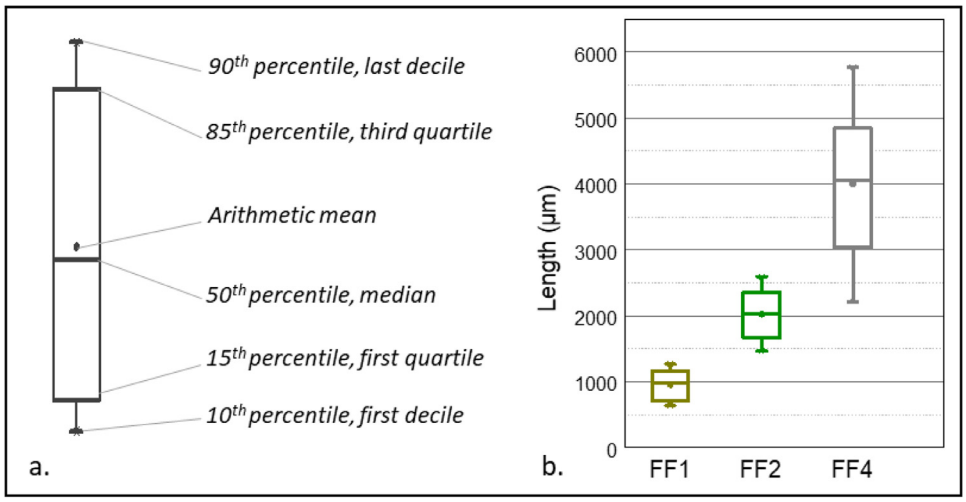

Fig. 2. a. Example of a box plot diagram and the appropriate signification, b. Length distribution of cut flax fibre samples of 1, 2 and 4 mm (samples FF1, FF2 and FF4, respectively) following scutching, and hackling.

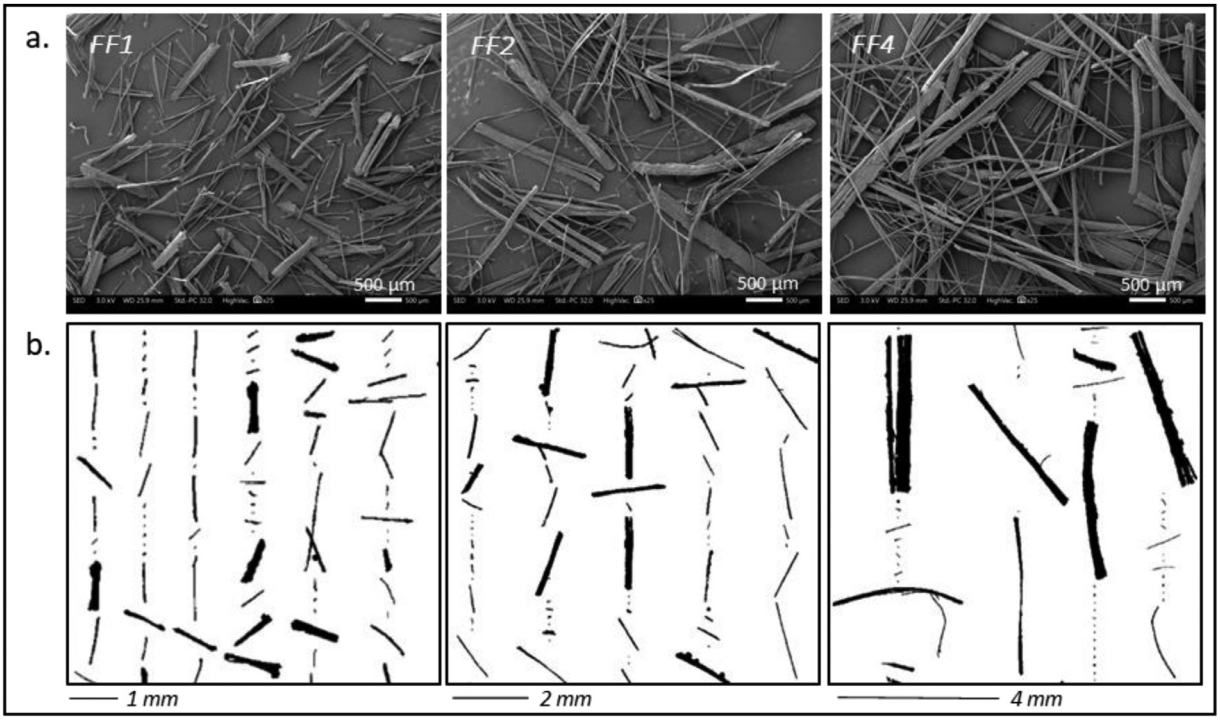

Fig. 3. a. SEM observations of cut flax fibre samples of 1, 2 and 4 mm (samples FF1, FF2 and FF4, respectively) following scutching, and hackling, b. Corresponding analysed particles obtained by dynamic image analysis.

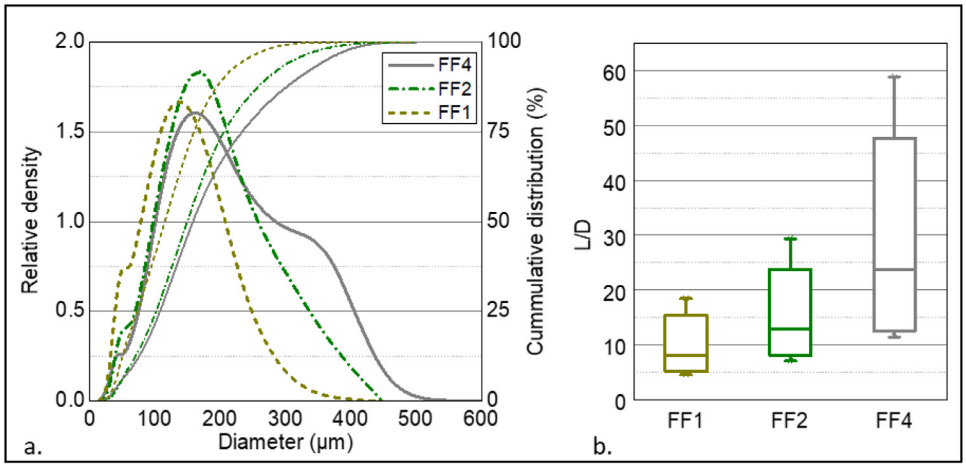

Fig. 4. a. Diameter cumulative (dotted line) and relative density (full line) distribution of the cut flax fibres. b. Aspect ratio distribution of the cut flax fibres.

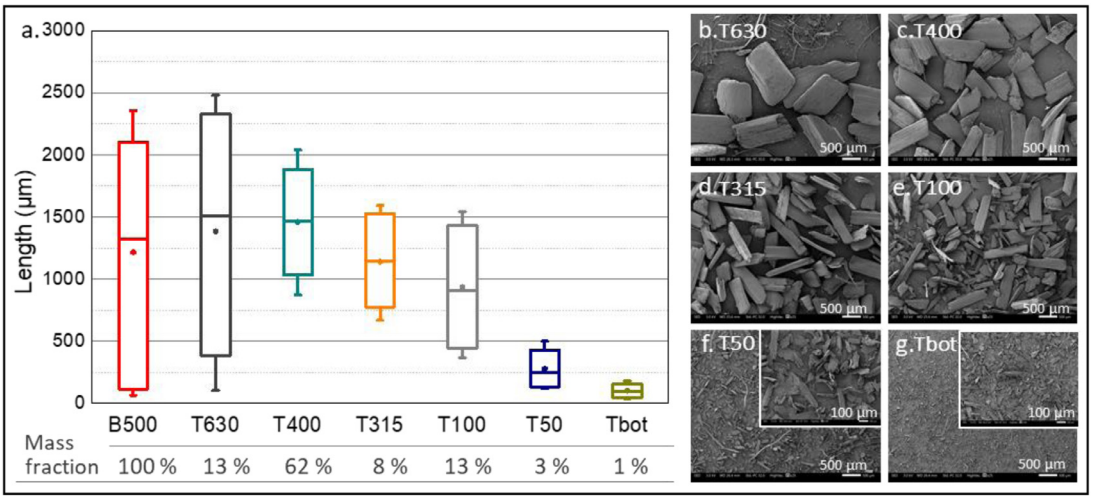

Fig. 5. a. Particle length distribution of flax shive samples before and after sieving with the corresponding mass fractions after sieving, b The SEM images of the sieved flax shives are taken with a x25 magnification for all samples except the T50 and Tbot detailed views, which are magnified at x100.

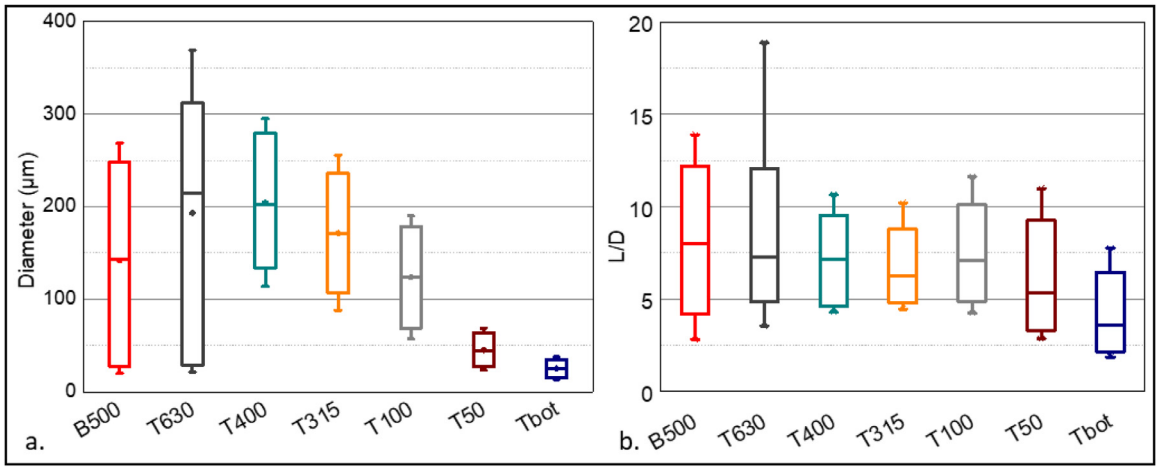

Fig. 6. a. Flax shive diameter distribution, b. Flax shive aspect ratio distribution.

sample T100 and to 1.7 for samples T50 and Tbot. While the particle length remarkably decreases for these three samples, the SEM images predictably show distinct heterogeneity in the particle length.

In this study, particle separation is conducted by means of a vibrating sieving device. Therefore, since a particle's aspect ratio increases with respect to a given mesh size, the probability of this particle passing through this specific sieve decreases [27]. Furthermore, the longest particles, which tend to agglomerate during sieving, and more fragmented particles can be found in sieve fractions like T50. The longest particles retained on the sieve tend to form a mesh and could agglomerate with smaller fragments, as observed for the T630 fraction containing both fibres and coarse particles. Agglomeration could also be due to static electricity charging of particles induced by repeated movements of the vibrating sieving operation.

Fig. 6a shows the evolution of the flax shives (FS) diameter with the sieving separation. The original fragmented FS sample, B500, shows a symmetric distribution, with a mean diameter of 142.4 ± 0.01 µm. The T630 sample, presenting the remaining unsieved particles, shows a particle diameter going from a first decile of 21.5 ± 0.3 µm to a last decile of 369 ± 85.7 µm, revealing the presence of both fibres and FS particles, with a mean diameter of 202.1 ± 20.4 µm. The following sieved fractions present a distribution close to symmetric, with a mean diameter that progressively decreases from 201.7 ± 18.0 µm for T400, 170.1 ± 4.9 µm for T315, 124.6 ± 0.3 µm for T100, 45.2 ± 1.2 µm for T50 and finally 25.5 ± 0.3 µm for the bottom sieve.

Interestingly, despite a substantial sieving time (over 40 min), the diameters of the particles overlap (Fig. 6a). This overlap can be explained by the fact that in order for particles to pass through a specific mesh size, they must have at least two dimensions that are inferior to the minimum square aperture of the given sieve [28]. Furthermore, during the dynamic image analysis method used, most particles can move freely in the three dimensions. This movement causes the measured "diameter" to potentially correspond to the particle's thickness. Flax shives, as seen in the SEM observations (Fig. 5b), have a rectangular shape when seen from all three dimensions.

The FS aspect ratio was additionally calculated and is given in Fig. 6b. A median aspect ratio of 8 for the initial fragmented FS sample (B500) decreases and stays relatively constant around 7 for samples T630, T400, T315 and T100, and then further decreases for the last two sieve fractions, at 5.4 and 3.6 for T50 and Tbot, respectively. The mean diameter decreases with respect to the decreasing mesh size, which is consistent with the decreasing aspect ratio of the particles.

Estimation of the morphological diversity of scutching and carding dust

For the two dust batches and associated fractions, SEM observations were performed (Fig. 7). The two batches, SD and CD, contain dust,

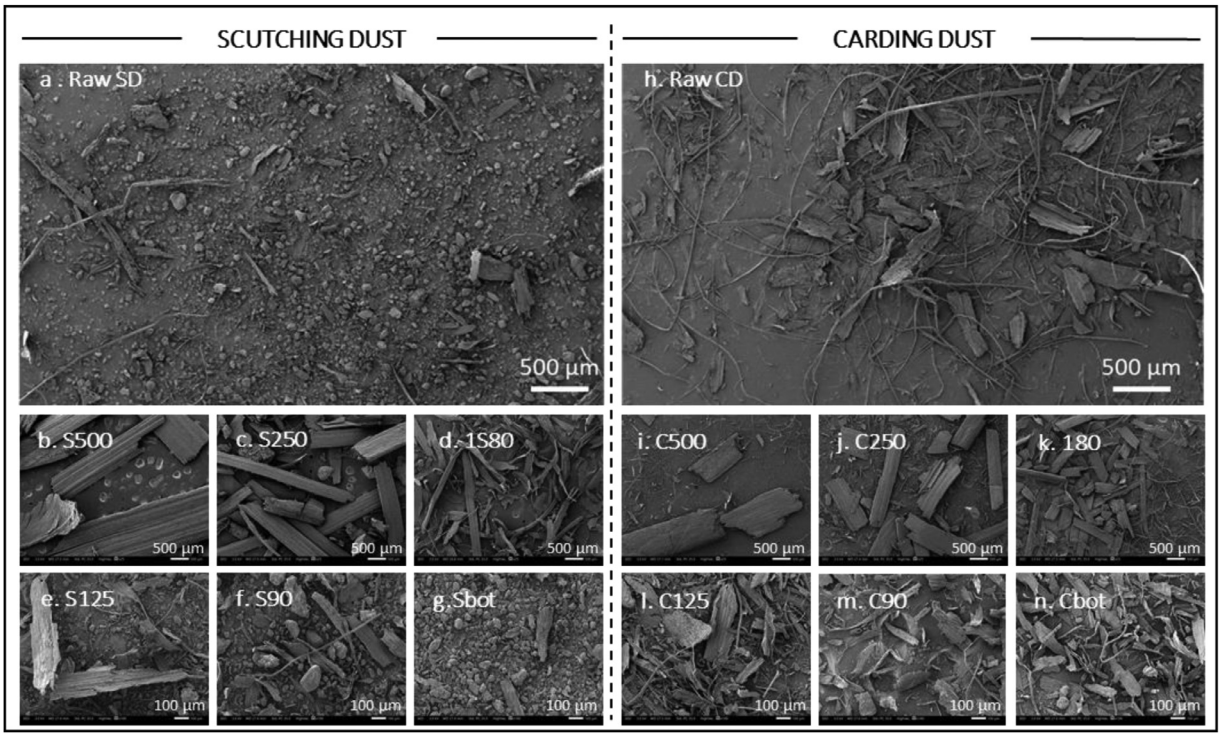

Fig. 7. SEM observation of; a. Scutching dust and h. Carding dust. Observations of each sieved fraction is shown in b-g and i-n sub-figures for scutching and carding dust, respectively, for each sieving grid: b, i = 500 µm, c, j = 250 µm, d, k = 180 µm, e, l = 125 µm, f, m = 90 µm and g, n = Tbot fraction.

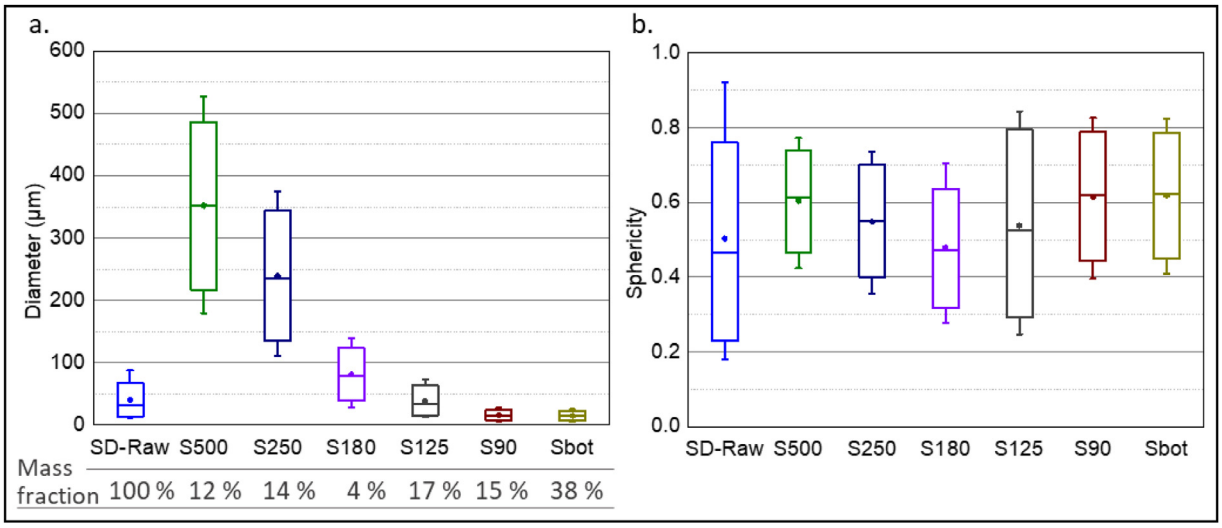

Fig. 8. a. Scutching dust diameter distribution, b. Scutching dust sphericity distribution.

fibres and shives at different proportions. One can notice that there are more fibres and shives for CD (Fig. 7h) in comparison with SD (Fig. 7a). Conversely, SD shows a greater dust population. This outcome is logical, as the carding stage takes place after scutching; at this stage, the batches of fibres have already been cleaned of almost all mineral pollution and of the shives and dust generated during scutching. Even if the shives are specifically sorted during scutching, a small fraction may be present in the scutching dust.

Fig. 8a shows the evolution of the diameter of the scutching dust (SD) as a function of the mesh of the sieve, and the resulting weight fractions are also mentioned. Concerning the SD-Raw sample, the dispersion is very low due to the important fraction of small particles in the raw batch (70%-wt < 125 μm), and the remaining fibres and shives poorly impact the results. As expected, an increase in the diameter is observed with an increase in the sieve mesh. The S500 sample has, with a symmetrical representation, the largest diameters, with an average diameter of 354.0 ± 11.6 μm and a last decile of 527.7 ± 22.0 μm, illustrating the presence of shive fragments, as evidenced in Fig. 7b. The S250 sample, with a first decile of 111.9 ± 7.1 μm and a last decile of 373.6 ± 30.1 μm, shows a mixture of shives and bundles of fibres (Fig. 7c). All of the following samples also have a distribution similar to a symmetrical distribution, the mean diameter of which decreases with a decrease in the size of the mesh of the sieves, with samples S180 and S125 having mean diameters of 81.6 ± 5.2 μm and 37.7 ± 1.3 μm, respectively. For the last two samples, S90 and Sbot, the dispersion of the diameters is much less pronounced. Indeed, the first decile is 6.2 ± 0.1 μm and the last decile is

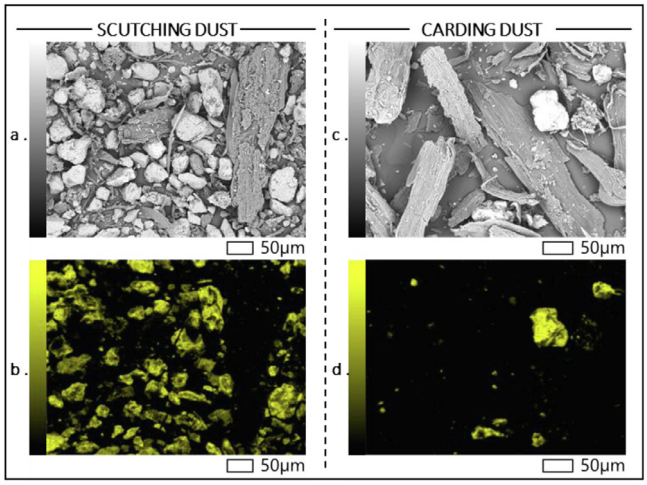

Fig. 9. a, c: initial SEM images of scutching and carding Tbot samples, respectively. b, d: silica analysis of the same respective samples via energy dispersive X-ray analyser (EDS).

28.0 ± 1.0 μm for sample S90. The trend is identical for the Sbot sample with a first decile of 6.3 ± 0.1 μm and a last decile of 25.5 ± 0.3 μm. These last two samples are representative of a mixture of dust and fibres. Fig. 7f and g strongly confirm this analysis with the presence of numerous small particles equivalent to fines, which probably come from mineral dust from the soil.

This hypothesis is confirmed by an elementary analysis, as shown in Fig. 9. Mainly found in the Sbot sample (Fig. 9a and b), these small particles are very rich in silica, which confirms their origin. They are present in much smaller quantities in the C-bot sample (Fig. 9c and d) due to the refining treatments undergone by the fibres, which have removed the majority of the soil residues.

Because the scutching and carding dust samples are both mainly composed of fines and because their morphology is quite different from that of fibres or shives, their sphericity was analysed rather than their aspect ratio, which would not really have a physical meaning in this case. Fig. 8b shows the sphericity of SD according to the mesh of the sieve, where a sphericity of one corresponds to a perfect sphere. The sphericity of SD-Raw presents the greatest dispersion: from 0.18 to 0.92. For all other samples, the sphericity oscillates between 0.25 and 0.84. However, some differences between the samples are noticeable. For S500 and S250, the dispersion of the sphericity is tight. Indeed, the first and last decile are 0.42 and 0.77, and 0.37 and 0.74 for S500 and S250, respectively. Samples S180 and S125 show the presence of particles with a sphericity less than 0.3 with a mean sphericity of 0.47 and 0.56, respectively. A fibre has a sphericity of approximately 0.3; therefore, this sphericity would suggest a significant presence of fibres in these two samples, as shown in Fig. 7d and e. Concerning the last two samples, S90 and Sbot, the first decile of the sphericity is very close to 0.40, with values of 0.39 and 0.40, respectively. These values indicate the presence of mainly dust and also of fibres, but in a lesser quantity.

Fig. 10a illustrates the evolution of the diameters of the carding dust (CD) as a function of the mesh of the sieves. A general decrease in the diameter is observed for each sample with decreasing sieve meshes. The C500 sample has a symmetrical diameter distribution, with a mean diameter of 235.1 ± 14.0 μm. The last decile of C500, 484.6 ± 22.7 μm, illustrates the presence of elongated particles like fibre bundles and/or shives (Fig. 7i). The C250 sample represents the diameters with a high dispersion towards large diameters: the value of the last decile is 295.7 ± 5.9 μm, showing the disappearance of the largest shives present in the C500 sample. In addition, the diameter distribution of the C250 sample is no longer symmetrical with a median diameter equal to 83.06 ± 1.7 μm. The last three samples (C125, C90 and Cbot) show a gradual decrease in the average diameter from 33.4 ± 0.8 μm for C125, 13.6 ± 0.2 μm for C90 and 13.2 ± 0.1 μm for Cbot. The C90 and Cbot samples mainly consist of dust and unit fibres (Fig. 7m and n). For the CD-Raw sample, the dispersion of diameters is very limited: from 10.2 ± 0.2 μm to 42.8 ± 1.3 μm; comprising the mean values obtained for samples C125, C90 and Cbot. One can notice in this case the very low fraction of dust, compared to SD sample at the same stage.

Fig. 10b shows the evolution of the sphericity of the samples following the sieving of CD. For the majority of the samples, the sphericity varies very little: 0.62, 0.66, 0.53 and 0.58 for samples C500, C250, C180 and C125, respectively. For the C90 and Cbot samples, the average sphericities are 0.53 and 0.55, respectively. In comparison with the reciprocal samples of the scutching dust (Sbot and S90), there is a decrease in this sphericity. In other words, it indicates the presence of more fibres in CD, whose sphericity is less than that of SD.

Fig. 11a shows the ash fractions of dry matter for the SD and CD. For raw samples (SD and CD), the difference is remarkable: the SD has an ash content of 58.2% for dry matter, whereas for the CD, the ash content does not exceed 8%. In this way, and SD is mainly made up of minerals. Fig. 11b also presents the distribution of the mass fraction of each sample, according to the size of the mesh of the various sieves used. The most important fraction of the SD originates from the Sbot sample

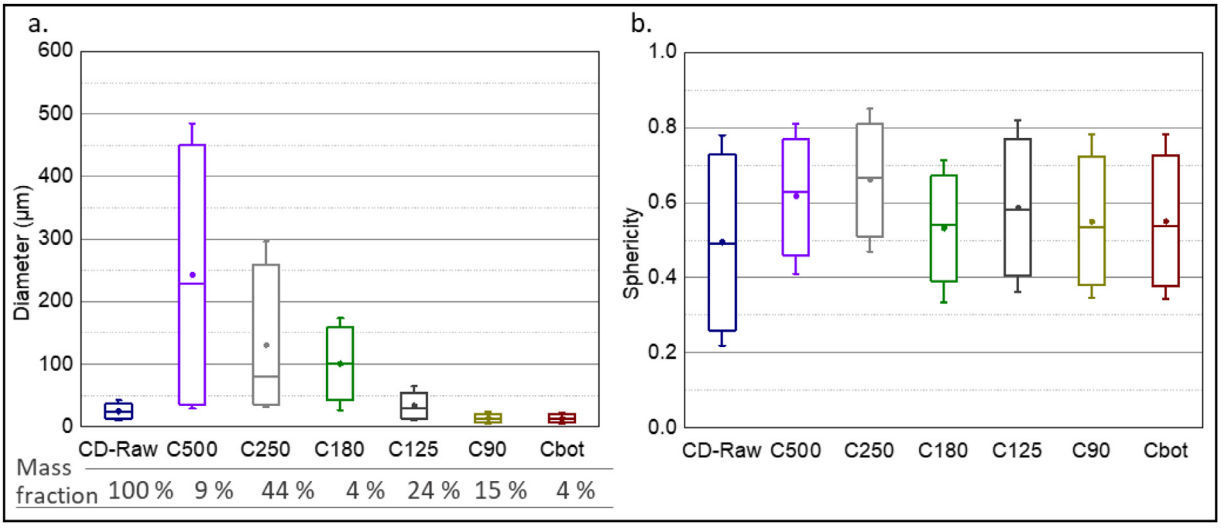

Fig. 10. a. Carding dust diameter distribution, b. Carding dust sphericity distribution.

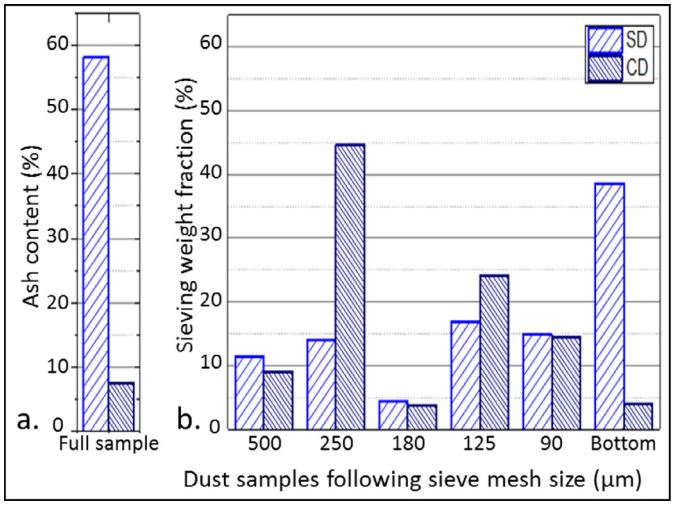

Fig. 11. a. Ash content scutching and carding dusts, b. Sieving mass fraction of SD and CD.

with 38% of the total mass, while the largest fraction of the CD corresponds to the 250 µm sieve (C250 sample) with almost 44% of the total mass. These distributions, specific to each type of dust originating from two distinct transformation processes, perfectly illustrate the diversity of the components making up the sample. Thus, CD is mainly made up of fibre elements (both elementary and in bundles) because the carding process occurs on tows obtained after the scutching process, where retted plant stems are mechanically transformed and are therefore also cleaned of the organic and mineral dusts they carry from the fields they were cultivated in.

Contribution in injection moulded composites

Reinforcing effect of the flax stem products

All three categories of reinforcing materials, for which the morphological aspects have been studied previously (Section 3.1), were used as reinforcement material at a 30% mass fraction, with the same poly(propylene) (PP) matrix containing 4%-wt maleic anhydride modified poly-(propylene) (MAPP) and processing conditions. The tensile behaviours of the injection moulded composites processed with each category of material (cut flax fibres FF1, fragmented flax shives B500, and both scutching SD and carding dust CD) are displayed in Fig. 12a, while Fig. 12b displays the Young's modulus of the different flax injection moulded composites as a function of the its tensile strength at break, and a comparison with the results obtained in the literature for other composites. The Fig. 12b shows that the scutching and carding dusts are already responsible for a + 24% and +32% increase in the Young's modulus, respectively, when compared to the initial PP-MAPP matrix, coming close to the flax fines studied by Bourmaud et al. [7], inducing a + 36% increase in the tensile modulus of the composite. The following are a + 88%, +112% and +114% increase in the Young's modulus due to wood flour (WF), B500 flax shives, and a 50/50-wt mixture of B500 flax shives and 1 mm-long flax fibres, respectively [21]. The action of 1 or 2 mm flax fibres induces an average +137% effect on the injection moulded composite's stiffness [7,21].

Concerning the effect of these reinforcing materials on the composite's strength at break, scutching dusts offer a limited, but nevertheless positive, 8% increase, while carding dusts and fines have an equivalent effect with a + 18% and +14% increase, respectively. Then, wood flour, B500 shives and the FF1-B500 mixture are responsible for an increase in strength of +48%, +39% and +53%, respectively. Finally, the fibre reinforcing materials (FF1 and FF2) are responsible for an increase in the tensile strength, ranging between +65% and +79%.

In addition to the expected increase in the tensile strength and Young's modulus, and a decrease in the deformation at break, the reinforcement materials do not change the global tensile behaviour of the reinforced PP-MAPP composites (Fig. 12a).

Furthermore, three categories (materialised by circles in Fig. 12b) of reinforcing efficiency, equivalent to the three types of materials presently studied can be differentiated: the fines, the particulate matter (fragmented shives or wood flour) and the fibres. These correspond to aspect ratios of less than or equal to 5 for the flax fines [7] and dusts, 5 to 8 for flax shives and 8 to 24 and above for the fibres studied here. Similarly, the reinforcement potential has also been observed for low aspect ratio fibres [29]. Nevertheless, an aspect ratio of 10 is generally admitted as the minimum in order to have a marked reinforcing effect in injection moulded composites, and this is only the case here for the flax fibre reinforced composites. One must nevertheless keep in mind that the method of analysis has an important impact on the absolute measured aspect ratio when comparing different literature sources. Manual methods are often imperfect due to their tendency to not take small particles with a low aspect ratio into account [9].

While the reinforcing potential of cut flax fibres in injection moulded composites greatly depends on their aspect ratio to transfer loads, the shearing stresses induced during the extrusion and injection steps are such that the fibre length is rapidly reduced by the transformation pro-

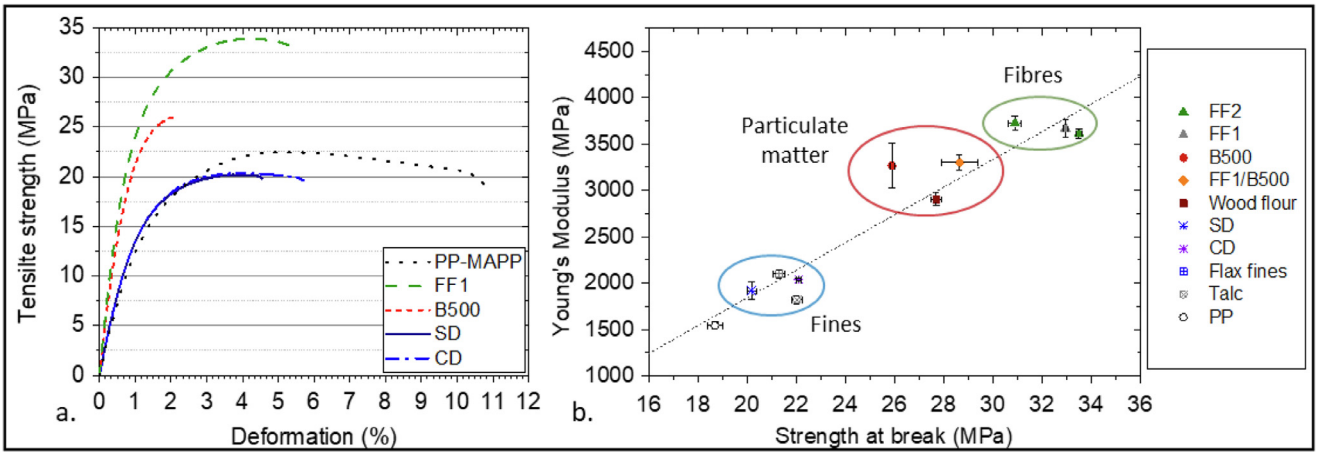

Fig. 12. a. Tensile behaviour of 30%-wt reinforcing materials in PP with 4%-wt MAPP, b. Young's modulus and tensile strength at break of a poly(propylene) injection moulded composite with 30%-wt of the reinforcement material. Data from 2 mm long flax fibres, flax fines and talc taken from [7], and that containing 1 mm flax fibres and flax shives or wood flour from [22].

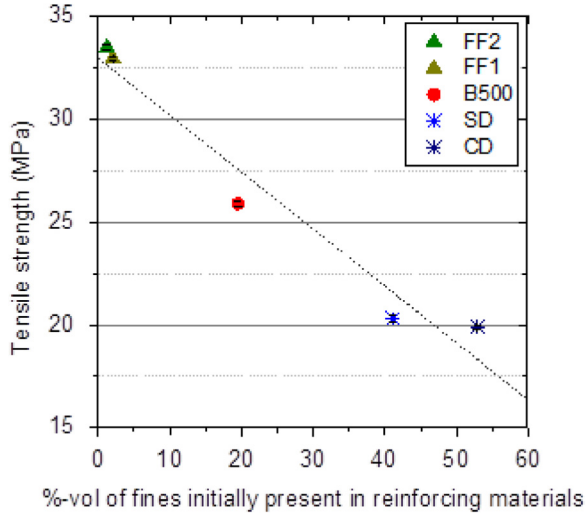

Fig. 13. Tensile strength at break as a function of fine particle content initially present in the reinforcing materials for injection moulded specimen.

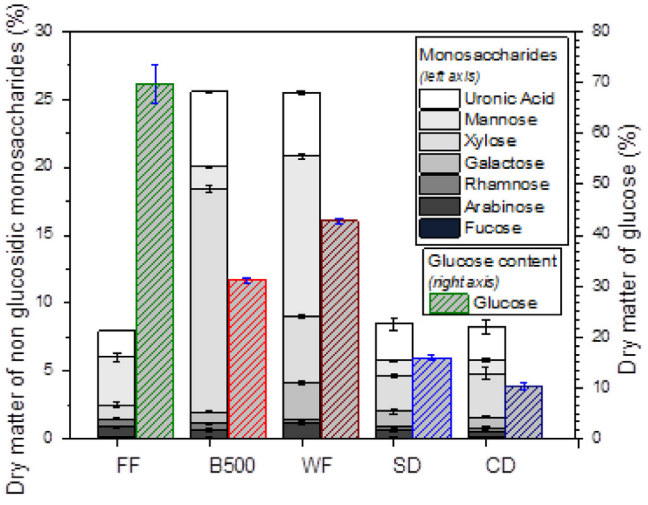

Fig. 14. Monosaccharides and glucose chemical composition of the main types of samples studied. WF refers to wood flour for comparison purposes. The FF, B500 and WF values have been completed from [22].

cess, either because of the fragile behaviour of the flax bundles, or by a fatigue mechanisms for elementary flax fibres [30]. For instance, it has been shown that 2 mm-long flax fibres have an equivalent reinforcing efficiency to 1 mm-long flax fibres in both the tensile strength and Young's modulus of poly-(propylene) injection moulded composites after the common extrusion and injection process steps, and at this stage both fibre samples had similar aspect ratios [31]. Interestingly, fines, CD and SD cannot be assimilated to just loading products, but have a real function of reinforcement, whether considering the strength or Young's modulus of associated composites. Even if their aspect ratio is moderate and also impacted by the extrusion and injection process, twin-screw extrusion is able to reach a high individualisation degree [3], in favour of the reinforcing effect, minimising the bundles and aggregates, even for low aspect ratio particles. The properties of both scutching and carding dusts are in agreement with both the tensile strength and tensile modulus values obtained with poplar sawdust, industrially used for wood plastic composite manufacturing, and PP and 2%-wt MAPP injection moulded composites where the reinforcement material has an aspect ratio between 3.5 and 4.5 [32].

As explained, the mechanical performances of these three families of flax reinforced composites are impacted by the aspect ratio of reinforcement; this latter is highly impacted by the volume fraction of fine particles (<200 μm), which here varies from 2% or less for all cut fibre lengths to 53% for the CD samples. Fig. 13 highlights a clear correlation ($R^2 = 0.974$) between the tensile strength at break and the volume fraction of fines initially present in the five categories of reinforcing samples.

These results confirm the strong impact of the L/D ratio on injection moulded composite mechanical properties. When exclusively analysing the population of fines originating from FF1 and FF2, their median aspect ratios are 2.8 and 2.5, respectively, while the median aspect ratios of the entire samples of cut fibres FF1 and FF2 are 8.2 and 13.1, respectively. Moreover, Bourmaud et al. [7] showed that the tensile strength at a break efficiency ratio of flax fines, generated by the fibre preparation process, is 1/10 when compared to 2 mm long flax fibres equivalent to the FF2 sample. Fines, and here more specifically dust, can be assimilated to fillers in their use in composite materials. The fillers have several roles, including that of reducing the cost of the material or increasing its processability by varying the stiffness or viscosity. It has been previously shown [7] that the apparent viscosity of PP-fine particles is similar to PP-talc. In addition, this apparent viscosity for high shear rates is relatively close to that of the virgin matrix, indicating the low impact of fines on the flow.

Furthermore, the mechanical properties of injection moulded depends on several parameters, such as the microstructure of the reinforcing materials, their distribution and orientation within the matrix, and on its the adherence with the matrix, to cite a few. As the totality of this information is not known in this study, the following discussion focuses on the known properties of the reinforcing materials.

Discussion on the carbohydrate composition

The results of the carbohydrate analysis carried out on the different sample categories are given in Fig. 14. Glucose, assimilated to cellulose, accounted for approximately 70% of flax fibre dry mass, while flax shives and wood flour (included here for comparison purposes) have a similar glucose content of 31 and 43%, respectively. The latter two samples also differentiate with their amount of xylose, which for flax shives is more than three times that of wood flour, and mannose content which, for wood flour, is 7 times that of flax shives. The wood flour data was taken from a previous study for comparative purposes [21] and sugar composition is in agreement with the literature [33]. It differs from the composition of the highly cellulosic flax fibres, whereas it is quite similar to that of flax shives. Due to crosslinking of the lignin-xylose network in wood cell walls, some authors [34] have evidenced an increase in the wood cell wall stiffness with the processing and recycling stage induced by temperature exposure. In this context, it would be interesting to further investigate the recycling behaviour of flax shives compounds. This could be a positive argument for developing these materials. Both the flax fibres' and flax shives' chemical compositions are in accordance with previous published studies [35,36].

Finally, the monosaccharide contents of the scutching and carding dusts are equivalent, with the exception of the glucose content, which is the lowest for CD at 10% against 16% for SD. In these fractions, a minor amount of broken fibres or shives appears to be present, which is consistent with the mineral ash contents measured by pyrolysis (Section 3.1.c).

The glucose content in the analysed reinforcing flax co-products is directly correlated with their reinforcing efficiency in PP-MAPP injection moulded composites, as seen in Fig. 15 by a linear relationship ($R^2 = 0.993$). The natural fibre cell walls are reinforced by cellulose organised in microfibrils, and their mechanical properties depend on the cellulose content, specific the microfibrillar angle (MFA) and its crystallisation degree [37]. The cellulose content is not significantly modified during the manufacturing process of injection moulded composites [38] at relatively low temperatures (cellulose and hemicelluloses begin to degrade above 250 °C [39]). This study therefore shows that the glu-

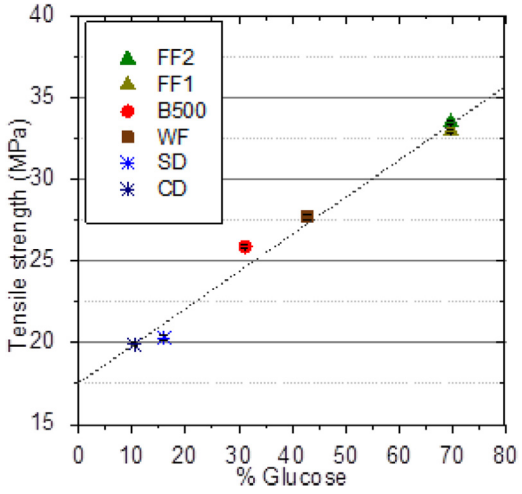

Fig. 15. Tensile strength at break as function of dry matter content of glucose in 30%-wt reinforced injection moulded specimen.

cose content is an accurate indicator of the reinforcing potential of flax stem products in injection moulded composites.

The present results confirm that carding dust has a better reinforcing potential than talc, which is similar to flax fines particles [7]. Regarding the scutching dust, the presence of numerous mineral particles (Fig. 9) can be problematic for transformation tools (screws, dies, channels, moulds) and cause premature breakage or wear. Nevertheless, by sieving (for example, by removing the mineral-rich 90 and Bot fractions in Fig. 7f and g), the quality of the batches and the aspect ratio of the reinforcements can be simply optimised. Thus, after minor improvements, dust can be viewed as a credible, eco-friendly, and low-cost alternative for mineral loading substitution in thermoplastic compounds.

Conclusion

This study focused on the relevant morphological parameters of a range of products obtained from the whole flax stem (flax fibres, flax shives, and dusts) with the aim of assessing their mechanical reinforcement potential for injection moulding applications. The dynamic image analysis used for this study delivered accurate information through a volume distribution analysis, particularly concerned with the three fibre batch lengths of 1 mm, 2 mm and 4 mm. The study of the particle diameter showed a slight decrease with the decrease in the fibre length due to more severe shear stresses during the cutting process. Fragmented flax shives have an aspect ratio of approximately 7.5, but a mass fraction concentrated at the coarser sized particles, namely, 62%-wt of particles between the 630 μm and 400 μm mesh-sized sieves. Furthermore, the dust samples originating from the scutching and the carding process, SD and CD, show very distinct morphological features, notably in terms of diameter, with much smaller mean diameters for the carding dust samples. Interestingly, the SD sample contains important amounts of silica, implying a larger volume of mineral particles originating from the crop cultivation fields. This larger volume is confirmed by considering the ash content of the two samples following pyrolysis.

In terms of the mechanical reinforcement, a strong correlation between the cellulose content of flax stem products or a fine particle content and maximum tensile strength was demonstrated. This outcome allows i) the reinforcing role of different biomass materials to be estimated based on the amount of cellulose, which is a stable criterion that does not significantly evolve during the manufacturing process and ii) the strong negative role of fines to be confirmed, especially due to their very low aspect ratios. Furthermore, flax shives and dusts have a very low-added value; their use as composite reinforcements is a potential additional income for scutching centres and also a way to increase the biomass fraction in thermoplastic composites by creating low-cost but competitive compounds in terms of their mechanical properties.

Declaration of Competing Interest

The authors declare that they have no known competing financial interests or personal relationships that could have appeared to influence the work reported in this paper.

Acknowledgements

The authors would like to thank the National Association of Research and Technology for financing a thesis in partnership with Van Robaeys Frères and the Dupuy de Lôme Research Institute of the South Brittany University (France). We would like to thank Sylviane Daniel (INRAE, Nantes) for her skilful help in the carbohydrate analysis, and Anthony Magueresse (IRDL, Lorient) for the SEM images. Furthermore, the authors would like to thank the Région Bretagne and Interreg V.A Cross-Channel Programme for funding this work through the FLOWER project (Grant number 23).

Supplementary materials

Supplementary material associated with this article can be found, in the online version, at doi:10.1016/j.jcomc.2020.100054.

References

[1] A. Bourmaud, J. Beaugrand, D.U. Shah, V. Placet, C. Baley, Towards the design of high-performance plant fibre composites, Prog. Mater. Sci. 97 (2018) 347–408, doi:10.1016/j.pmatsci.2018.05.005.
[2] K. Haag, et al., Influence of flax fibre variety and year-to-year variability on composite properties, Ind. Crops Prod. 98 (2017) 1–9, doi:10.1016/j.indcrop.2016.12.028.
[3] A.S. Doumbia, et al., Flax/polypropylene composites for lightened structures: multiscale analysis of process and fibre parameters, Mater. Des. 87 (2015) 331–341, doi:10.1016/j.matdes.2015.07.139.
[4] A. Kelly, W.R. Tyson, Tensile properties of fibre-reinforced metals: copper/tungsten and copper/molybdenum, J. Mech. Phys. Solids 13 (1965) 329–350.
[5] G. Coroller, et al., Effect of flax fibres individualisation on tensile failure of flax / epoxy unidirectional composite, Compos. Part A Appl. Sci. Manuf. 51 (2013) 62–70, doi:10.1016/j.compositesa.2013.03.018.
[6] A. Bourmaud, D. Åkesson, J. Beaugrand, A. Le Duigou, M. Skrifvars, C. Baley, Recycling of L-poly-(lactide)-poly-(butylene-succinate)-flax biocomposite, Polym. Degrad. Stab. 128 (2016) 77–88, doi:10.1016/j.polymdegradstab.2016.03.018.
[7] A. Bourmaud, C. Mayer-Laigle, C. Baley, J. Beaugrand, About the frontier between filling and reinforcement by fine flax particles in plant fibre composites, Ind. Crops Prod. 141 (September) (Dec. 2019) 111774, doi:10.1016/j.indcrop.2019.111774.
[8] C. Mayer-Laigle, A. Bourmaud, D.U. Shah, N. Follain, J. Beaugrand, Unravelling the consequences of ultra-fine milling on physical and chemical characteristics of flax fibres, Powder Technol. 360 (2020) 129–140, doi:10.1016/j.powtec.2019.10.024.
[9] N. Le Moigne, M. Van Den Oever, T. Budtova, A statistical analysis of fibre size and shape distribution after compounding in composites reinforced by natural fibres, Composits Part A 42 (10) (2011) 1542–1550, doi:10.1016/j.compositesa.2011.07.012.
[10] K. Haag, J. Müssig, Scatter in tensile properties of flax fibre bundles: influence of determination and calculation of the cross- sectional area, J. Mater. Sci. 51 (2016) 7907–7917, doi:10.1007/s10853-016-0052-z.
[11] J. Müssig, H.G. Schmid, Quality control of fibers along the value added chain by using scanning technique – from fibers to the final product, Microsc. Microanal. 10 (S02) (Aug. 2004) 1332–1333, doi:10.1017/S1431927604884320.
[12] J. Müssig, S. Amaducci, Scanner based image analysis to characterise the influence of agronomic factors on hemp (Cannabis sativa L.) fibre width, Ind. Crops Prod. 113 (2018) 28–37 December 2017, doi:10.1016/j.indcrop.2017.12.059.
[13] L. Teuber, H. Militz, A. Krause, Dynamic particle analysis for the evaluation of particle degradation during compounding of wood plastic composites, Composits Part A Appl. Sci. Manuf. 84 (2016) 464–471, doi:10.1016/j.compositesa.2016.02.028.
[14] F. Berzin, J. Beaugrand, S. Dobosz, T. Budtova, B. Vergnes, Lignocellulosic fiber breakage in a molten polymer. Part 3. Modeling of the dimensional change of the fibers during compounding by twin screw extrusion, Compos. Part A Appl. Sci. Manuf. 101 (2017) 422–431 https://doi.org/, doi:10.1016/j.compositesa.2017.07.009.
[15] S.E. Hamdi, C. Delisée, J. Malvestio, N. Da Silva, A. Le Duc, J. Beaugrand, X-ray computed microtomography and 2D image analysis for morphological characterization of short lignocellulosic fibers raw materials: a benchmark survey, Compos. Part A Appl. Sci. Manuf. 76 (2015) 1–9, doi:10.1016/j.compositesa.2015.04.019.
[16] F. Berzin, B. Vergnes, J. Beaugrand, Evolution of lignocellulosic fibre lengths along the screw profile during twin screw compounding with polycaprolactone, Compos. Part A Appl. Sci. Manuf. 59 (2014) 30–36, doi:10.1016/j.compositesa.2013.12.008.

[17] M. Graça Carvalho, P.J. Ferreira, A.A. Martins, M. Margarida Figueiredo, A comparative study of two automated techniques for measuring fiber length, Tappi J. 80 (2) (1997) 137–142, doi:10.1201/9781420038064.ch4.
[18] D. Guay, et al., Comparison of fiber length analyzers, in: Proceedings of the 2005 TAPPI Practical Papermaking Conference, 2005, pp. 413–442.
[19] J. Meyers, H. Nanko, Effects of fines on the fiber length and coarseness values measured by the Fiber Quality Analyzer (FQA), in: Proceedings of the 2005 TAPPI Practical Papermaking Conference, 2005, pp. 383–397.
[20] N. Martin, P. Davies, C. Baley, Comparison of the properties of scutched flax and flax tow for composite material reinforcement, Ind. Crops Prod. 61 (2014) 284–292, doi:10.1016/j.indcrop.2014.07.015.
[21] L. Nuez, et al., The potential of flax shives as reinforcements for injection moulded polypropylene composites, Ind. Crop. Prod. 148 (March) (2020) 112324, doi:10.1016/j.indcrop.2020.112324.
[22] A.B. Blakeney, P.J. Harris, R.J. Henry, B.A. Stone, A simple and rapid preparation of alditol acetates for monosaccharide analysis, Carbohydr. Res. 113 (2) (1983) 291–299, doi:10.1016/0008-6215(83)88244-5.
[23] N. Blumenkrantz, G. Asboe-Hansen, New method for quantitative determination of uronic acids, Anal. Biochem. 54 (2) (1973) 484–489.
[24] K. Albrecht, T. Osswald, E. Baur, T. Meier, S. Wartzack, J. Müssig, Fibre length reduction in natural fibre-reinforced polymers during compounding and injection moulding—experiments versus numerical prediction of fibre breakage, J. Compos. Sci. 2 (2) (2018) 20, doi:10.3390/jcs2020020.
[25] A. Le Duc, B. Vergnes, T. Budtova, Polypropylene/natural fibres composites: analysis of fibre dimensions after compounding and observations of fibre rupture by rheo-optics, Compos. Part A Appl. Sci. Manuf. 42 (11) (2011) 1727–1737, doi:10.1016/j.compositesa.2011.07.027.
[26] M. Tanguy, A. Bourmaud, J. Beaugrand, T. Gaudry, C. Baley, Polypropylene reinforcement with flax or jute fibre; Influence of microstructure and constituents properties on the performance of composite, Compos. Part B Eng. 139 (2018) 64–74 November 2016, doi:10.1016/j.compositesb.2017.11.061.
[27] J.C. Ludwick, P.L. Henderson, Particle shape and inference of size from sieving, Sedimentology 11 (3–4) (1968) 197–235, doi:10.1111/j.1365-3091.1968.tb00853.x.
[28] T. Allen, Powder Sampling and Particle Size Determination, Elsevier B.V., 2003.
[29] A. Bourmaud, S. Pimbert, Investigations on mechanical properties of poly(propylene) and poly(lactic acid) reinforced by miscanthus fibers, Compos. Part A Appl. Sci. Manuf. 39 (9) (2008) 1444–1454, doi:10.1016/j.compositesa.2008.05.023.
[30] R. Castellani, et al., Lignocellulosic fiber breakage in a molten polymer. Part 1. Qualitative analysis using rheo-optical observations, Compos. Part A Appl. Sci. Manuf. 91 (2016) 229–237, doi:10.1016/j.compositesa.2016.10.015.
[31] G. Ausias, A. Bourmaud, G. Coroller, C. Baley, Study of the fibre morphology stability in polypropylene-flax composites, Polym. Degrad. Stab. 98 (6) (2013) 1216–1224, doi:10.1016/j.polymdegradstab.2013.03.006.
[32] A. Nourbakhsh, A. Karegarfard, A. Ashori, A. Nourbakhsh, Effects of particle size and coupling agent concentration on mechanical properties of particulate-filled polymer composites, J. Thermoplast. Compos. Mater. 23 (2) (2010) 169–174, doi:10.1177/0892705709340962.
[33] R.C. Pettersen, The chemical composition of wood, in: The Chemistry of Solid Wood, CRC Press, 1985, pp. 57–126.
[34] L. Soccalingame, A. Bourmaud, D. Perrin, J.-C. Bénézet, A. Bergeret, Reprocessing of wood flour reinforced polypropylene composites: impact of particle size and coupling agent on composite and particle properties, Polym. Degrad. Stab. 113 (2015) 72–85, doi:10.1016/j.polymdegradstab.2015.01.020.
[35] A.U. Buranov, G. Mazza, Extraction and characterization of hemicelluloses from flax shives by different methods, Carbohydr. Polym. 79 (1) (2010) 17–25, doi:10.1016/j.carbpol.2009.06.014.
[36] C. Mayer-Laigle, R. Rajaonarivony, N. Blanc, X. Rouau, Comminution of dry lignocellulosic biomass: part II. Technologies, improvement of milling performances, and security issues, Bioengineering 5 (3) (2018) 1–17, doi:10.3390/bioengineering5030050.
[37] A. Bourmaud, C. Morvan, A. Bouali, V. Placet, P. Perré, C. Baley, Relationships between micro-fibrillar angle , mechanical properties and biochemical composition of flax fibers, Ind. Crop. Prod. 44 (2013) 343–351, doi:10.1016/j.indcrop.2012.11.031.
[38] C. Gourier, A. Le Duigou, A. Bourmaud, C. Baley, Mechanical analysis of elementary flax fibre tensile properties after different thermal cycles, Compos. Part A Appl. Sci. Manuf. 64 (2014) 159–166, doi:10.1016/j.compositesa.2014.05.006.
[39] D. Siniscalco, O. Arnould, A. Bourmaud, A. Le Duigou, C. Baley, Monitoring temperature effects on flax cell-wall mechanical properties within a composite material using AFM, Polym. Test. 69 (April) (2018) 91–99, doi:10.1016/j.polymertesting.2018.05.009.